


**Amyloid Inhibitors** Hot Paper

 How to cite: *Angew. Chem. Int. Ed.* **2025**, e202422834  
 doi.org/10.1002/anie.202422834

# Multi-Targeting Macrocyclic Peptides as Nanomolar Inhibitors of Self- and Cross-Seeded Amyloid Self-Assembly of $\alpha$ -Synuclein

*Simon Hornung, Dominik P. Vogl, Denise Naltsas, Beatrice Dalla Volta, Markus Ballmann, Beatrice Marcon, Muhammed Muazzam Kamil Syed, Yiyang Wu, Anna Spanopoulou, Regina Feederle, Luzia Heidrich, Jürgen Bernhagen, Thomas Koeglsperger, Günter U. Höglinger, Gerhard Rammes, Hilal A. Lashuel, and Aphrodite Kapurniotu\**

**Abstract:** Amyloid self-assembly of  $\alpha$ -synuclein ( $\alpha$ Syn) is linked to the pathogenesis of Parkinson's disease (PD). Type 2 diabetes (T2D) has recently emerged as a risk factor for PD. Cross-interactions between their amyloidogenic proteins may act as molecular links. In fact, fibrils of islet amyloid polypeptide (IAPP) (T2D) can cross-seed  $\alpha$ Syn amyloidogenesis and  $\alpha$ Syn and IAPP colocalize in PD brains. Inhibition of both self- and IAPP-cross-seeded  $\alpha$ Syn amyloidogenesis could thus interfere with PD pathogenesis. Here we show that macrocyclic peptides, designed to mimic IAPP self-/cross-interaction sites and previously found to inhibit amyloidogenesis of IAPP and/or Alzheimer's disease (AD) amyloid- $\beta$  peptide A $\beta$ 40(42), are nanomolar inhibitors of both self- and IAPP-cross-seeded amyloid self-assembly of  $\alpha$ Syn. Anti-amyloid function is mediated by nanomolar affinity interactions with  $\alpha$ Syn via three  $\alpha$ Syn regions which are identified as key sites of both  $\alpha$ Syn self-assembly and its cross-interactions with IAPP. We also show that the peptides block A $\beta$ 42-mediated cross-seeding of  $\alpha$ Syn as well. Based on their broad spectrum anti-amyloid function and additional drug-like features, these peptides are leads for multifunctional anti-amyloid drugs in PD, T2D, AD, and their comorbidities, while the identified  $\alpha$ Syn key segments are valuable targets for novel, multi-site targeting amyloid inhibitors in PD and related synucleinopathies.

[\*] Dr. S. Hornung, Dr. D. P. Vogl, M. Sc. D. Naltsas, Dr. B. D. Volta, M. Sc. B. Marcon, Dr. A. Spanopoulou, M. Sc. L. Heidrich, Prof. Dr. A. Kapurniotu  
 Division of Peptide Biochemistry  
 TUM School of Life Sciences  
 Technische Universität München (TUM)  
 Emil-Erlenmeyer-Forum 5, D-85354 Freising, Germany  
 E-mail: akapurniotu@tum.de

M. Sc. M. Ballmann, Prof. Dr. G. Rammes  
 Department of Anesthesiology and Intensive Care  
 Technische Universität München (TUM)/Klinikum Rechts der Isar  
 Ismaningerstr. 22, D-81675 Munich, Germany

M. Sc. M. M. K. Syed, Prof. H. A. Lashuel  
 Laboratory of Molecular and Chemical Biology of Neurodegeneration  
 École Polytechnique Fédérale de Lausanne (EPFL)  
 CH 1015 Lausanne, Switzerland

M. Sc. Y. Wu, PD. Dr. T. Koeglsperger, Prof. Dr. G. U. Höglinger  
 Department of Neurology  
 LMU University Hospital, Ludwig-Maximilian-University (LMU),  
 Marchioninstr. 15, D-81377 Munich, Germany  
 and  
 German Center for Neurodegenerative Diseases (DZNE)  
 Feodor-Lynen-Straße 17, D-81377 Munich, Germany  
 and  
 Munich Cluster for Systems Neurology (SyNergy)  
 Feodor-Lynen-Straße 17, D-81377 Munich, Germany

Dr. R. Feederle  
 Core Facility Monoclonal Antibodies  
 Helmholtz Center Munich German Research Center  
 for Environmental Health  
 Ingolstädter Landstr. 1, D-85764 Neuherberg, Germany  
 and  
 Munich Cluster for Systems Neurology (SyNergy)  
 Feodor-Lynen-Straße 17, D-81377 Munich, Germany  
 and  
 German Center for Neurodegenerative Diseases (DZNE) Feodor-  
 Lynen-Straße 17, D-81377 Munich, Germany

Prof. Dr. J. Bernhagen  
 Division of Vascular Biology  
 Institute for Stroke and Dementia Research (ISD)  
 LMU University Hospital, Ludwig-Maximilian-University (LMU)  
 Feodor-Lynen-Straße 17, D-81377 Munich, Germany  
 and  
 Munich Cluster for Systems Neurology (SyNergy)  
 Feodor-Lynen-Straße 17, D-81377 Munich, Germany

Dr. D. P. Vogl  
 Current address: Boehringer Ingelheim, Vienna, Austria

Dr. A. Spanopoulou  
 Current address: ITM Isotope Technologies Munich SE  
 Garching/Munich, Germany

M. Sc. L. Heidrich  
 Current address: Life & Brain GmbH, Bonn, Germany

© 2025 The Author(s). Angewandte Chemie International Edition published by Wiley-VCH GmbH. This is an open access article under the terms of the Creative Commons Attribution License, which permits use, distribution and reproduction in any medium, provided the original work is properly cited.

## Introduction

Aberrant amyloid self-assembly is linked to the pathogenesis of more than 50 devastating diseases.<sup>[1]</sup> These include Parkinson's disease (PD), the second most common neurodegenerative disease after Alzheimer's disease (AD), and type 2 diabetes (T2D), which affect more than 10 and 450 million people worldwide, respectively.

The key amyloid protein in PD is the 140-residue presynaptic protein  $\alpha$ -synuclein ( $\alpha$ Syn), while the key amyloid polypeptide of T2D is the 37-residue islet amyloid polypeptide (IAPP) (Scheme 1).<sup>[1b]</sup> In PD brains, large amounts of neurotoxic  $\alpha$ Syn oligomers and fibrils are present both in intraneuronal inclusions and extracellularly, mediating inflammation, neurodegeneration, and transmission of pathology.<sup>[2]</sup> In T2D, IAPP aggregates into cytotoxic oligomers and amyloid fibrils in the pancreas; these assemblies underlie inflammation,  $\beta$ -cell degeneration, and T2D pathogenesis.<sup>[3]</sup> Under physiological conditions however, IAPP, which is secreted from the pancreatic  $\beta$ -cells and is present both in blood and in brain, functions as a neuroendocrine regulator of glucose homeostasis.<sup>[3]</sup>

Increasing evidence suggests that T2D is a risk factor for PD.<sup>[4]</sup> Thereby, cross-interactions between  $\alpha$ Syn and IAPP have been suggested to act as a possible molecular link between the two diseases.<sup>[5]</sup> In fact, in vitro studies showed that IAPP fibrils (fIAPP) are able to act as “cross-

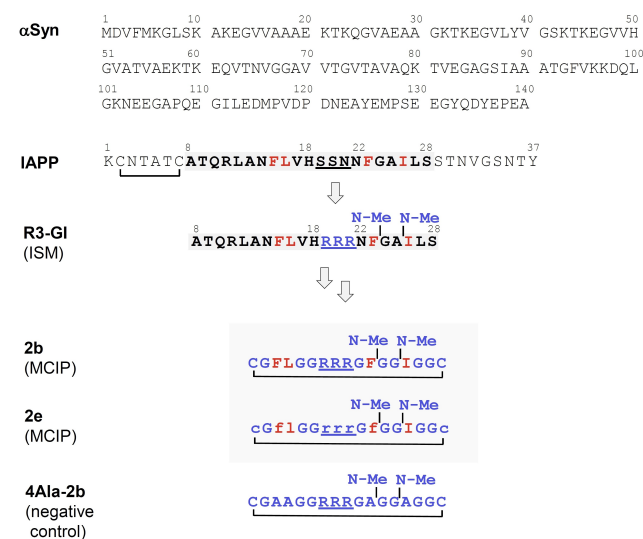
seeds”, thus strongly accelerating  $\alpha$ Syn amyloid self-assembly and these findings were recently confirmed by in vivo studies with PD mouse models.<sup>[5a,c]</sup> Additional support for a potential pathogenic relevance of  $\alpha$ Syn/IAPP cross-interactions for PD includes evidence for  $\alpha$ Syn/IAPP co-aggregates in brains of PD patients and for  $\alpha$ Syn deposits in the pancreas of PD and T2D patients, and the emerging role of  $\alpha$ Syn cross-interactions and cross-seeding events in cell-to-cell spreading of  $\alpha$ Syn pathology in PD and related synucleinopathies.<sup>[5c,d,6]</sup>

Based on the above, devising inhibitors of both self- and fIAPP-cross-seeded amyloid self-assembly of  $\alpha$ Syn could be a reasonable approach to suppress PD pathogenesis, in particular also in PD/T2D comorbidity. However, both  $\alpha$ Syn and IAPP are intrinsically disordered proteins (IDPs) and cross-interaction sites and structures of their hetero-assemblies are yet unknown, making amyloid inhibitor design a difficult task.<sup>[7]</sup> In fact, none of the reported  $\alpha$ Syn amyloid inhibitors or pipeline PD therapeutics including antibodies, peptides, and small molecules has yet advanced into the clinic or was shown to suppress cross-seeding of  $\alpha$ Syn; PD is a still incurable disease.<sup>[8]</sup>

Macrocyclic peptides are highly attractive drug candidates.<sup>[9]</sup> The reason is that they can combine, in addition to their own favorable features, key drug-like properties of antibodies and small molecules.<sup>[9]</sup> Their properties may thus include high potency, high affinity, target selectivity, and the large surface area often required for inhibitors of protein-protein (or IDP/IDP) interactions including anti-amyloid molecules.<sup>[9–10]</sup> Furthermore, macrocyclic peptides may exhibit, or become engineered to feature, proteolytic stability and BBB permeability, two highly desirable properties for PD anti-amyloid drugs.<sup>[9–11]</sup>

Previous studies showed that IAPP/amyloid- $\beta$  peptide (A $\beta$ 40(42)) cross-amyloid interaction sites can be used to design peptides as potent inhibitors of their amyloid self-assembly and cross-seeding interactions.<sup>[7d,11–12,14]</sup> In this context, we have previously designed the IAPP-derived macrocyclic peptides **2b** and **2e** as nanomolar inhibitors of amyloid self-assembly of both IAPP and AD's A $\beta$ 40(42) (**2b**) or A $\beta$ 40(42)-only (**2e**).<sup>[7d,11]</sup> The two 17-residue peptides (termed macrocyclic inhibitory peptides or MCIPs) were designed to mimic IAPP surfaces mediating self- and/or cross-interactions with A $\beta$ 40(42) while maintaining a minimum amount of recognition elements (Scheme 1).<sup>[7d,11]</sup> MCIP design was based on the IAPP amyloid core segment IAPP(8–28), containing key recognition elements for both IAPP self-assembly and its cross-interactions with A $\beta$ , and an IAPP(8–28) analog, the linear peptide R3-GI termed IAPP interaction surface mimic (ISM) (Scheme 1).<sup>[11–13,15]</sup> Importantly, MCIP **2e**, which differs from **2b** only in the presence of D- instead L-amino acids, exhibited high proteolytic stability in human plasma in vitro and BBB-crossing ability in a cell model, making it a lead for AD anti-amyloid drugs.<sup>[7d,11]</sup>

Here we show that macrocyclic peptides **2b** and **2e** are nanomolar inhibitors of both self- and fIAPP-cross-seeded  $\alpha$ Syn amyloid self-assembly. In addition, we show that their



**Scheme 1.** Sequences of  $\alpha$ Syn, IAPP, and the previously designed linear template peptide R3-GI (IAPP interaction surface mimic or ISM; IAPP-based sequence numbering), macrocyclic inhibitory peptides (**2e** and **2b**), and negative control peptide **4Ala-2b** (Supporting Tables S1, S2).<sup>[11–12]</sup> All peptides including IAPP are C-terminal amides.<sup>[11–12]</sup> IAPP amyloid core IAPP(8–28) is in bold and highlighted in grey; IAPP(19–21), which is replaced by RRR or rrr in IAPP(8–28)-derived peptides, and RRR or rrr segments are underlined (D-amino acids, lower case letters). Colour code: red for the 4 key residues of IAPP self-/cross-interactions with A $\beta$  and blue for non-IAPP residues and amide bond N-methyl groups (N–Me).<sup>[11–13]</sup> IAPP contains a disulfide bridge between Cys2 and Cys7 and the MCIPs between Cys1 and Cys17.<sup>[11]</sup>

potent anti-amyloid function is mediated by nanomolar affinity binding to  $\alpha$ Syn via 3  $\alpha$ Syn segments which are identified as key sites of both  $\alpha$ Syn self-assembly and its cross-interactions with IAPP and that the two peptides also block cross-seeding of  $\alpha$ Syn by A $\beta$ 42 fibrils (fA $\beta$ 42).

## Results and Discussion

### Nanomolar Affinity IAPP/ $\alpha$ Syn Cross-Interactions Mediated by IAPP Amyloid Core Region IAPP(8–28)

We first determined the IAPP regions that mediate its cross-interactions with  $\alpha$ Syn. Synthetic peptide arrays containing IAPP decamers covering full-length IAPP and positionally shifted by one residue were incubated with biotin-labeled  $\alpha$ Syn (Biotin- $\alpha$ Syn) and Biotin- $\alpha$ Syn-bound decamers were visualized by chemiluminescence.<sup>[15a]</sup> We found a major cluster of 4 consecutive decamers within IAPP(8–20), while a second weaker cluster localized in

IAPP(13–27) (Figure 1a, Supporting Figure S1). We then titrated synthetic N<sup>6</sup>-terminal fluorescein-labeled IAPP (Fluos-IAPP) and IAPP(8–28) (Fluos-IAPP(8–28)) with  $\alpha$ Syn. This method capitalizes on the dependence of the fluorescence emission of a fluorophore on its local environment and its change upon ligand binding which correlates with the extent of complex formation.<sup>[16]</sup> Binding of  $\alpha$ Syn to the labeled peptides resulted in an  $\alpha$ Syn concentration-dependent fluorescence enhancement (Figure 1b, c). This enhancement could be due to the increased rigidity of the fluorophore in the hetero-complex. Sigmoidal titration curves were obtained and yielded low nanomolar apparent (app.)  $K_d$  values of 26.7 ( $\pm$ 6.0) nM for the Fluos-IAPP/ $\alpha$ Syn interaction and 8.2 ( $\pm$ 2.3) nM for the Fluos-IAPP(8–28)/ $\alpha$ Syn interaction (means ( $\pm$ SD), 3 assays) (Figure 1b, c). This data revealed that IAPP binds  $\alpha$ Syn with low nanomolar affinity and that the IAPP amyloid core IAPP(8–28) contains the key recognition elements for the IAPP/ $\alpha$ Syn interaction as earlier found for the IAPP/IAPP and the IAPP/A $\beta$ 40(42) interactions.<sup>[13,15a]</sup>

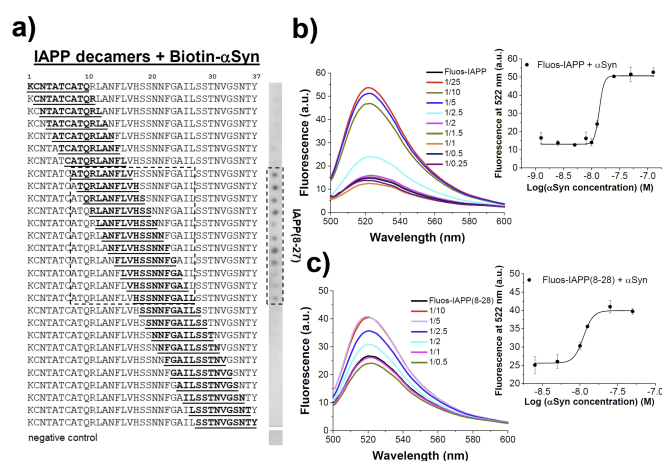


**Figure 1.** Identification of IAPP regions that interact with  $\alpha$ Syn by using peptide arrays (a) and determination of the binding affinities of interactions of  $\alpha$ Syn with IAPP and IAPP(8–28) by fluorescence spectroscopic titrations (b,c). a) Synthetic peptide arrays containing IAPP decamers (bold & underlined) were incubated with Biotin- $\alpha$ Syn (0.5  $\mu$ M); decamers which bound Biotin- $\alpha$ Syn are in dashed rectangles. Array representative of two arrays synthesized in parallel and two independent incubations with Biotin- $\alpha$ Syn. b,c) Fluorescence emission spectra of Fluos-IAPP (b) and Fluos-IAPP(8–28) (c) (5 nM) alone or their mixtures with various molar ratios of  $\alpha$ Syn (Fluos-peptide/ $\alpha$ Syn) as indicated; data from 1 representative assay out of 3. Insets show binding curves; data means ( $\pm$ SD) of 3 titration assays.

### Macrocyclic Peptides **2b** and **2e** are Nanomolar Inhibitors of Self- and IAPP-Cross-Seeded Amyloid Self-Assembly of $\alpha$ Syn

Based on the above, we hypothesized that the IAPP(8–28)-derived macrocyclic peptides **2b** and **2e** might mimic IAPP/ $\alpha$ Syn cross-interaction surfaces and interfere with  $\alpha$ Syn amyloid self-assembly and its cross-seeding by fIAPP. Notably, initial studies showed that both IAPP(8–28), which is intrinsically amyloidogenic, and its non-amyloidogenic analogs IAPP(8–28)-GI and R3-GI, two linear MCIP precursors, were unable to inhibit  $\alpha$ Syn fibrillogenesis (Scheme 1, Supporting Table S1, Supporting Figure S2).<sup>[11–12,17]</sup>

The effects of **2b** and **2e** on  $\alpha$ Syn amyloid self-assembly were then studied (Scheme 1, Figure 2a–c, Table 1). In parallel, we studied the effects of the negative control peptide **4Ala-2b** in which all four IAPP-derived key residues of **2b** and **2e** were replaced by Ala (Scheme 1).<sup>[11]</sup> According to the amyloid specific Thioflavin T (ThT) binding assay and transmission electron microscopy (TEM),  $\alpha$ Syn fibrillogenesis started after a lag-time of ~24 h and was apparently completed at ~48 h (Figure 2a, b & Supporting Figure S3a–c). However, in the presence of **2b** or **2e** ( $\alpha$ Syn/peptide 1/1) a full suppression of  $\alpha$ Syn fibrillogenesis was observed (Figures 2a, b & Supporting Figure S3b,c). In addition, **2b** and **2e** strongly suppressed

**Table 1:** IC<sub>50</sub> of inhibitory effects of **2b**, **2e**, and **4Ala-2b** on cell-damaging effects of un-seeded, f $\alpha$ Syn-seeded, and fIAPP-cross-seeded  $\alpha$ Syn amyloid self-assembly.

Peptide	IC <sub>50</sub> ( $\pm$ SD) (nM) Inhibition of $\alpha$ Syn <sup>[a]</sup>	IC <sub>50</sub> ( $\pm$ SD) (nM) Inhibition of $\alpha$ Syn + f $\alpha$ Syn <sup>[a]</sup>	IC <sub>50</sub> ( $\pm$ SD) (nM) Inhibition of $\alpha$ Syn + fIAPP <sup>[a]</sup>
<b>2b</b>	62.3 ( $\pm$ 33.9)	51.8 ( $\pm$ 4.8)	75.2 ( $\pm$ 21.1)
<b>2e</b>	66.0 ( $\pm$ 23.3)	54.7 ( $\pm$ 4.4)	42.0 ( $\pm$ 18.5)
<b>4Ala-2b</b>	> 5000	> 5000	> 5000

[a] IC<sub>50</sub> values, means ( $\pm$ SD) from 3 titration assays ( $n=3$  wells each);  $\alpha$ Syn, 100 nM w/o or with preformed f $\alpha$ Syn or fIAPP seeds (10%).

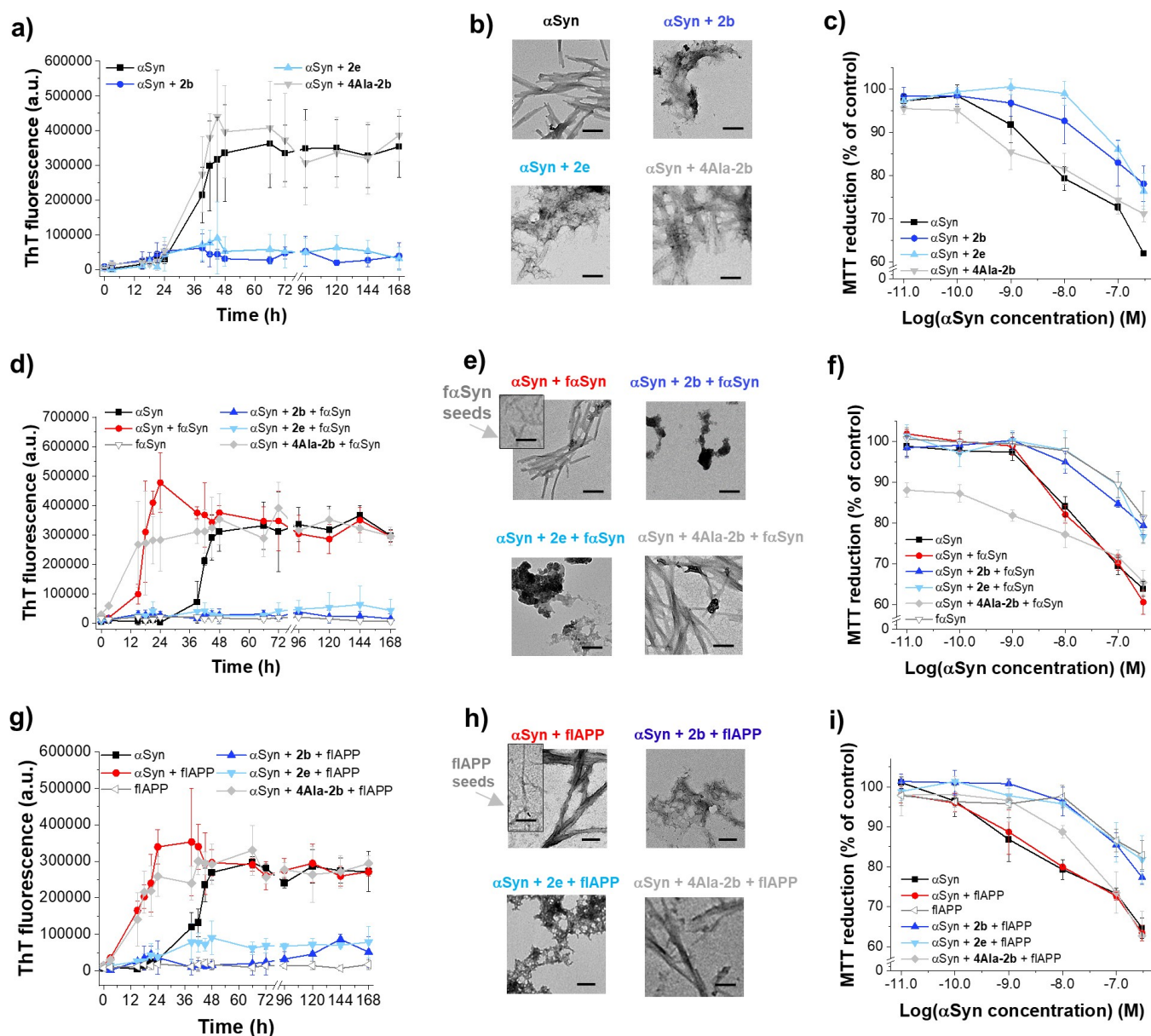


**Figure 2.** Effects of **2b**, **2e**, and **4Ala-2b** on non-seeded (a–c), seeded with preformed  $f\alpha$ Syn (d–f), and flAPP-cross-seeded  $\alpha$ Syn amyloid self-assembly and related cell-damaging effects (g–i). a–c) Fibrillogenesis of  $\alpha$ Syn (3  $\mu$ M) alone or in the presence of **2b** and **2e** (1/1) or **4Ala-2b** (1/50) determined by ThT binding (means ( $\pm$ SD), 3 assays (3 wells each)) (a); TEM images of solutions (7 day-aged) from (a) as indicated (color code as in (a)) (scale bars, 100 nm) (b); PC12 cell viability after treatment with solutions from (a) (7 day-aged) determined by the MTT reduction assay (means ( $\pm$ SD), 3 assays (3 wells each)) (c). d–f) Fibril formation of  $\alpha$ Syn alone (3  $\mu$ M) or seeded by preformed  $f\alpha$ Syn (10%) alone or with **2b** and **2e** (1/1) or **4Ala-2b** (1/50) as determined by the ThT binding assay and ThT binding of  $f\alpha$ Syn seeds (0.3  $\mu$ M) (means ( $\pm$ SD), 3 assays (3 wells each)) (d); TEM images of solutions from (d) aged for 7 days (seeded  $\alpha$ Syn/**2b**(**2e**) mixtures) or for 24 h (seeded  $\alpha$ Syn alone or with **4Ala-2b**) and from  $f\alpha$ Syn seeds (scale bars, 100 nm) (e); PC12 cell viability after treatment solutions from (d) (7 day-aged) determined by the MTT reduction assay (means ( $\pm$ SD), 3 assays (3 wells each)) (f). g–i) Fibrillogenesis of  $\alpha$ Syn (3  $\mu$ M) alone or cross-seeded by flAPP (10%) alone or with **2b** and **2e** (1/1) or **4Ala-2b** (1/50) determined by ThT binding and ThT binding of flAPP seeds (0.3  $\mu$ M) (means ( $\pm$ SD), 3 assays (3 wells each)) (g); TEM images of solutions from (g) aged for 7 days (cross-seeded  $\alpha$ Syn/**2b**(**2e**)) or for 24 hours (cross-seeded  $\alpha$ Syn alone or with **4Ala-2b**) as indicated (scale bars, 100 nm) (h); PC12 cell viability after treatment with solutions from (g) (7 day-aged) determined by the MTT reduction assay (means ( $\pm$ SD), 3 assays (3 wells each)) (i).

formation of cell-damaging  $\alpha$ Syn assemblies according to the 3-[4,5-dimethylthiazol-2-yl]-2,5-diphenyltetrazolium bromide (MTT) reduction assay in cultured rat pheochromocytoma (PC12) cells (Figure 2c, Supporting Figure S3d,e). In fact,  $\alpha$ Syn titrations with **2b** and **2e** revealed

nanomolar IC<sub>50</sub> values, i.e. 62.3 ( $\pm$ 33.9) nM (**2b**) and 66.0 ( $\pm$ 23.3) nM (**2e**) (Table 1, Supporting Figure S3d,e). No attenuating effects were found for the negative control **4Ala-2b** up to a 50-fold higher molar excess than **2b** or **2e** (Figure 2a–c).

We next asked whether **2b** and **2e** might also suppress seeding of  $\alpha$ Syn fibrillogenesis by preformed  $\alpha$ Syn fibrils (f $\alpha$ Syn). Addition of f $\alpha$ Syn seeds (10%) to  $\alpha$ Syn strongly accelerated formation of  $\alpha$ Syn fibrils and cell-damaging aggregates as expected (Figure 2d–f, Supporting Figure S4). However, in the presence of **2b** and **2e** (1/1),  $\alpha$ Syn fibrillogenesis and cell toxicity were fully suppressed whereas again **4Ala-2b** ( $\alpha$ Syn/**4Ala-2b**, 1/50) did not inhibit (Figure 2d–f, Supporting Figure S4). Titrations with the two inhibitors yielded IC<sub>50</sub> values of 51.8 ( $\pm$ 4.8) nM (**2b**) and 54.7 ( $\pm$ 4.4) nM (**2e**) which were nearly identical to the IC<sub>50</sub> values of effects on unseeded  $\alpha$ Syn fibrillogenesis (Table 1, Supporting Figure S5). Notably, **2b** and **2e** inhibited  $\alpha$ Syn fibrillogenesis and cytotoxicity when seeding was performed both with 10% and 1% f $\alpha$ Syn seeds, indicative of effects on secondary nucleation and fibril elongation events (Figure 2d–f, Supporting Figure S4–S6).<sup>[18]</sup>

We then asked whether the two peptides might also interfere with the cross-seeding effect of IAPP fibrils (fIAPP) on  $\alpha$ Syn fibrillogenesis.<sup>[5a]</sup> Addition of seed amounts (10%) of preformed IAPP fibrils (fIAPP) to  $\alpha$ Syn strongly accelerated its fibrillogenesis consistent with previous findings (Figure 2g, h).<sup>[5a]</sup> In parallel, a strong acceleration of formation of cell-damaging  $\alpha$ Syn species was also observed (Supporting Figure S7a,b). Importantly, in the presence of **2b** or **2e** (1/1) a full suppression of cross-seeding of  $\alpha$ Syn fibrillogenesis and cytotoxicity was found and titrations yielded nanomolar IC<sub>50</sub> values for both peptides, i.e. 75.2 ( $\pm$ 21.1) nM (**2b**) and 42.0 ( $\pm$ 18.5) nM (**2e**) (Table 1, Supporting Figure S7c–h). As expected, **4Ala-2b** (50-fold) did not inhibit (Figure 2g–i). Notably, **2b** and **2e** were non-amyloidogenic and non-cytotoxic up to at least 200-fold higher concentrations than the IC<sub>50</sub> values consistent with the design concept and previous results (Supporting Figure S8).<sup>[11–12,19]</sup>

Taken together, the above studies identified MCIPs **2b** and **2e** as nanomolar inhibitors of both self- and fIAPP-cross-seeded amyloid self-assembly of  $\alpha$ Syn.

### MCIPs Bind $\alpha$ Syn with Nanomolar Affinity and Sequester it into Non-Fibrillar and Non-Cytotoxic Co-Assemblies

To learn more about the inhibition mechanism,  $\alpha$ Syn/peptide interactions and co-assemblies were studied by various biophysical and biochemical methods. First, the affinities of  $\alpha$ Syn/peptide interactions were determined by fluorescence spectroscopic titrations of synthetic N-terminal fluorescein-labeled **2b** (Fluos-**2b**) and **2e** (Fluos-**2e**) with  $\alpha$ Syn (Figure 3a, b). Low nanomolar app. K<sub>d</sub> values were obtained for both interactions (Fluos-**2b**/ $\alpha$ Syn, app. K<sub>d</sub>=17.2 ( $\pm$ 2.6) nM; Fluos-**2e**/ $\alpha$ Syn app. K<sub>d</sub>=22.0 ( $\pm$ 5.1) nM) in good agreement with the IC<sub>50</sub> values (Figure 3a, b, Tables 2 & 1). Of note, **2b** and **2e** were mostly monomeric at low nanomolar concentrations but self-assembled into soluble oligomers at higher concentrations as expected from their design concept and previous findings (Supporting Figure S9).<sup>[11–12,20]</sup> Also, their  $\alpha$ Syn binding affinities were very similar to their IAPP binding affinities while **4Ala-2b** did not bind either IAPP or  $\alpha$ Syn (Supporting Figure S10, S11, Table 2).<sup>[11]</sup>

The far-UV CD spectrum of freshly dissolved  $\alpha$ Syn exhibited a pronounced minimum at ~200 nm indicative of mainly disordered structure consistent with previous reports (Figure 3c, d).<sup>[21]</sup> Following aging for 48 h, a marked reduction of the CD magnitude was observed indicative of  $\alpha$ Syn oligomerization.<sup>[21a,b]</sup> In the presence of **2b** or **2e**, however, no/slower reduction of the CD magnitude was observed in line with their inhibitory activity on  $\alpha$ Syn amyloid self-assembly (Figure 3c, d). Also, in addition to the minimum at ~200 nm, the CD spectra of  $\alpha$ Syn/inhibitor mixtures exhibited a weaker but clear minimum between 220–230 nm. Their shapes and magnitudes suggested that hetero-complexes were more ordered than  $\alpha$ Syn (Figure 3c, d).

Next,  $\alpha$ Syn/inhibitor hetero-complexes were cross-linked with glutaraldehyde and following separation by SDS-PAGE visualized by western blot (WB) with anti- $\alpha$ Syn and anti-**2e**(**2b**) antibodies (Figure 3e & Supporting Figure S12). In freshly made  $\alpha$ Syn solutions, monomers and dimers were major species; trimers and other medium-to-high MW aggregates tended to be less abundant.<sup>[21c]</sup> In  $\alpha$ Syn/**2b**(**2e**) mixtures, a similar pattern as in  $\alpha$ Syn alone was observed with the difference that the bands stained with both the anti- $\alpha$ Syn and a monoclonal anti-**2e**(**2b**)

**Table 2:** App. K<sub>d</sub>s of interactions of Fluos-**2b**, -**2e**, and -IAPP with IAPP,  $\alpha$ Syn, and the three identified  $\alpha$ Syn key segments determined by fluorescence spectroscopic titrations.<sup>[a]</sup>

Binding partner	App. K <sub>d</sub> ( $\pm$ SD) (nM) ( <b>2b</b> )	App. K <sub>d</sub> ( $\pm$ SD) (nM) ( <b>2e</b> )	AApp. K <sub>d</sub> ( $\pm$ SD) (nM) (IAPP)
IAPP	29.6 ( $\pm$ 19.3)	46.9 ( $\pm$ 33.4)	9.7 ( $\pm$ 0.9) <sup>[19]</sup>
$\alpha$ Syn	17.2 ( $\pm$ 2.6)	22.0 ( $\pm$ 5.1)	26.7 ( $\pm$ 6.0)
$\alpha$ Syn(1–14)	366.2 ( $\pm$ 115.8)	461.3 ( $\pm$ 47.5)	886.4 ( $\pm$ 552.0)
$\alpha$ Syn(34–52)	662.8 ( $\pm$ 9.4)	504.7 ( $\pm$ 171.2)	347.5 ( $\pm$ 103.2)
$\alpha$ Syn(87–105)	72.1 ( $\pm$ 20.5)	122.2 ( $\pm$ 17.1)	31.9 ( $\pm$ 0.6)

[a] App. K<sub>d</sub>s, means ( $\pm$ SD) from 3 binding curves (3 titration assays) using N<sup>α</sup>-terminal fluorescein-labeled **2b** (Fluos-**2b**), **2e** (Fluos-**2e**), and IAPP (Fluos-IAPP) (pH 7.4). Fluos-peptides 5 nM except for titrations of Fluos-**2b**(**2e**) with  $\alpha$ Syn and of Fluos-IAPP with IAPP (data from ref. [19]) (Fluos-peptides 1 nM).<sup>[19]</sup>

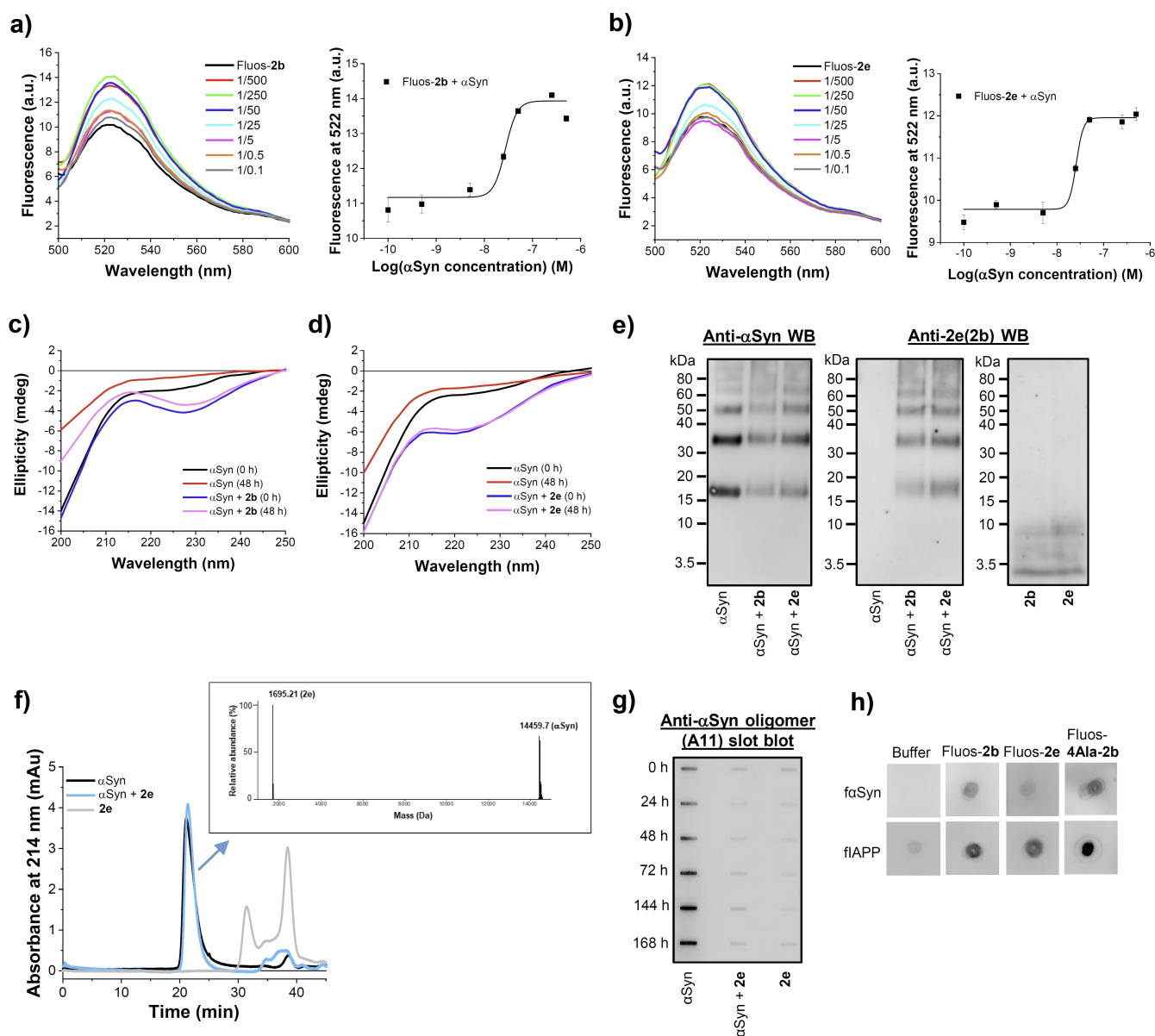


**Figure 3.** Studies on interactions, hetero-complexes, and mechanism of inhibitory effects of **2e** and **2b** on  $\alpha$ Syn amyloid self-assembly. a, b) Left, app.  $K_d$ s of interactions of Fluos-**2b** (a) and Fluos-**2e** (b) with  $\alpha$ Syn determined by fluorescence spectroscopic titrations. Fluorescence emission spectra of Fluos-**2b** or Fluos-**2e** (1 nM) and their mixtures with various molar ratios of  $\alpha$ Syn are shown as indicated; spectra from 1 representative binding assay out of 3. Right side, binding curves; data means ( $\pm$ SD) of 3 titration assays; app.  $K_d$ s in Table 2. c, d) Far-UV CD spectra of  $\alpha$ Syn (1  $\mu$ M) alone and its mixtures with **2b** (c) or **2e** (d) (10  $\mu$ M) measured at 0 h and after 48 h of incubation. e) Characterization of  $\alpha$ Syn/MCIP hetero- and  $\alpha$ Syn homo-oligomers by cross-linking with glutaraldehyde, SDS-PAGE, and western blot with anti- $\alpha$ Syn (left) or anti-**2e(2b)** (right) antibodies ( $\alpha$ Syn, 10  $\mu$ M; MCIPs, 50  $\mu$ M) antibody (see also Supporting Figure S12); representative results from 3 assays. f) Characterization of  $\alpha$ Syn/**2e** hetero-complexes in comparison to  $\alpha$ Syn and **2e** alone by size exclusion chromatography (SEC). Chromatograms of  $\alpha$ Syn (3  $\mu$ M), **2e** (30  $\mu$ M), and the  $\alpha$ Syn/**2e** mixture (1/10) are shown. Inset, ESI-MS spectrum (deconvoluted) of the 21 min peak from SEC of the  $\alpha$ Syn/**2e** mixture (see also Supporting Figure S14). Determined MWs as indicated; calculated mass (average) 14460.27 Da ( $\alpha$ Syn) and 1695.04 Da (**2e**). Representative results from 3 SEC analyses and ESI-MS. g) Kinetics of  $\alpha$ Syn self-assembly into A11-reactive toxic oligomers alone or in the presence of **2e** followed by slot blot analysis using the A11 antibody (see also Supporting Figure S15). Solutions  $\alpha$ Syn (3  $\mu$ M) alone,  $\alpha$ Syn/**2e** (1/1), and **2e** (3  $\mu$ M) alone were analyzed at indicated incubation time points. Representative results from 4 assays. h) Binding of **2b**, **2e**, and **4Ala-2b** to  $\alpha$ Syn and flAPP determined by dot blot analysis. Fluos-**2b**, Fluos-**2e**, and Fluos-**4Ala-2b** (1.5  $\mu$ M) and the buffer alone control were incubated with membranes containing spotted  $\alpha$ Syn or flAPP; binding was visualized by fluorescence (see also Supporting Figure S16). Representative results from 3 assays.

antibody; in addition, bands corresponding to  $\alpha$ Syn mono-, di-, and trimers were slightly shifted upwards. This data indicated that **2b** and **2e** co-assemble with  $\alpha$ Syn monomers

and low MW oligomers into hetero-dimers and low MW hetero-oligomers.

Hetero-complexes formed at early steps of  $\alpha$ Syn/**2e** co-assembly were then studied by size exclusion chromatography (SEC) (Figure 3f).  $\alpha$ Syn monomers (~15 kDa) present in freshly made  $\alpha$ Syn alone solutions eluted at a retention time ( $t_R$ ) of ~21 min corresponding to a globular protein of ~44 kDa; this was due to its natively unfolded nature resulting in a higher hydrodynamic radius (Figure 3f, Supporting Figure S13).<sup>[21a,b]</sup> In **2e** alone (~2 kDa) solutions, the major fraction eluted at ~38 min and corresponded to **2e** monomers while a smaller fraction corresponding to **2e** oligomers eluted at ~32 min. Importantly, in the  $\alpha$ Syn/**2e** mixtures, the 21 min peak found in  $\alpha$ Syn alone was still present but the **2e** alone peaks were strongly diminished (Figure 3f). These findings were consistent with formation of  $\alpha$ Syn/**2e** hetero-complexes which eluted at ~21 min and were confirmed by electrospray ionization mass spectrometry (ESI-MS) (Figure 3f, Supporting Figure S14). The observed lack of a shift of the  $\alpha$ Syn peak to higher MWs in the  $\alpha$ Syn/**2e** mixture was most likely due to the low MW of **2e** and the resolution limit of the column. Together, the above studies suggested  $\alpha$ Syn/**2e** hetero-dimers and low MW hetero-oligomers as early species in the  $\alpha$ Syn/**2e** co-assembly pathway.

Formation of cytotoxic  $\alpha$ Syn oligomers is associated with neurodegeneration and PD pathogenesis.<sup>[22]</sup> Our ThT binding and MTT reduction assays suggested that in the presence of the MCIPs formation of cytotoxic assemblies of  $\alpha$ Syn was strongly suppressed (Figure 2a–c). To characterize the effects of MCIPs on formation of  $\alpha$ Syn oligomers more directly, we followed kinetics of cytotoxic oligomer formation in  $\alpha$ Syn alone and its mixtures with **2e**. We used slot blot analysis and the antibody A11 reported to recognize toxic oligomers of various different proteins including  $\alpha$ Syn (Figure 3g, Supporting Figure S15a).<sup>[23]</sup> Formation of cytotoxic  $\alpha$ Syn oligomers was further confirmed by MTT reduction and TEM (Supporting Figure S15b–e). In  $\alpha$ Syn alone, good amounts of cytotoxic A11-reactive oligomers were present in ~48 h-aged solutions (Figure 3g, Supporting Figure S15). By contrast, significantly lower amounts of A11-reactive oligomers and no cytotoxic effects were observed in the  $\alpha$ Syn/**2e** mixtures (1/1) (Figure 3g, Supporting Figure S15a, b).

The potent inhibitory activity of the MCIPs could also be mediated by binding to  $\alpha$ Syn and/or IAPP resulting in suppression of secondary nucleation and/or fibril elongation.<sup>[18]</sup> In fact, dot blot assays showed that Fluos-**2b** and Fluos-**2e** are able to bind both  $\alpha$ Syn and IAPP (Figure 3h). However, the non-inhibitor Fluos-**4A1a-2b** also bound -most likely non-specifically-(Figure 3h, Supporting Figure S16). In addition, sub-stoichiometric amounts of **2b** and **2e** did not markedly affect self-/cross-seeded  $\alpha$ Syn fibrillogenesis (Supporting Figure S3, S5, S7). Furthermore,  $\alpha$ Syn/**2e**(**2b**) hetero-complexes were unable to become (cross-)seeded by  $\alpha$ Syn or IAPP consistent with a key role in MCIPs' anti-amyloid function (Supporting Figure S17, S18).

In conclusion, the anti-amyloid effects of **2b** and **2e** on  $\alpha$ Syn are likely mediated by high affinity interactions between monomeric and/or oligomeric states of MCIPs and

$\alpha$ Syn resulting in  $\alpha$ Syn sequestration into amorphous, non-cytotoxic, and non-(cross-)seedable  $\alpha$ Syn/MCIP co-assemblies. Interestingly, a similar mechanism has been suggested to underlie inhibitory effects of MCIPs and related IAPP-derived inhibitors on amyloid self-assembly of IAPP and A $\beta$ 40(42).<sup>[11–12,14a,20]</sup>

### Additional Anti-Amyloid Effects of the MCIPs

The impairment of hippocampal synaptic long term potentiation (LTP) by  $\alpha$ Syn oligomers is believed to be directly linked to neuronal dysfunction in PD.<sup>[2a,24]</sup> To obtain first information about the potential physiological relevance of our in vitro findings, we investigated the effects of the two MCIPs on  $\alpha$ Syn oligomer-mediated impairment of hippocampal synaptic LTP in mouse brains ex vivo (Figure 4a–c). In fact, electrophysiological studies showed that synaptic LTP damage caused by preformed cytotoxic  $\alpha$ Syn oligomers was significantly reduced by **2b** or **2e** (Figure 4a–c, Supporting Figure S19).<sup>[24a]</sup> Effects of the MCIPs on  $\alpha$ Syn toxicity were also studied using  $\alpha$ Syn overexpressing postmitotic dopaminergic Lund human mesencephalic (LUHMES) neurons, a previously developed disease-relevant cell model for the screening of putative modulators of  $\alpha$ Syn toxicity.<sup>[25]</sup>  $\alpha$ Syn cytotoxicity was quantified by the lactate dehydrogenase (LDH) release assay. Importantly, significant protection of the neurons was found for both peptides providing additional support for their anti-amyloid function (Figure 4d). In addition, as A $\beta$ -mediated cross-seeding of  $\alpha$ Syn may play a role in AD/PD co-pathology we asked whether **2b** and **2e**, found to also inhibit A $\beta$  amyloid self-assembly, may affect this process as well.<sup>[26]</sup> In fact, ThT binding, TEM, and cell viability studies revealed a full suppression of fA $\beta$ 42-cross-seeding of  $\alpha$ Syn in their presence (1/1) (Figure 4e–g). Finally, ThT binding studies showed that **2b** and **2e** do not inhibit insulin fibrillogenesis although their precursors IAPP and IAPP-GI were found to inhibit this process (Supporting Figure S20).<sup>[14c]</sup> Since **2b** inhibits amyloid self-assembly of A $\beta$ 40(42), IAPP, and  $\alpha$ Syn whereas **2e** inhibits A $\beta$ 40(42) and  $\alpha$ Syn but not IAPP, our findings support the notion that the anti-amyloid multifunctionality of the two peptides is target-selective.<sup>[11]</sup> Studies with additional putative interaction partners will be required to further address this issue.

### Three $\alpha$ Syn Key Regions Mediate its High Affinity Interactions with both the MCIPs and IAPP: Multi-Site Binding Underlies MCIP Anti-Amyloid Function

To identify  $\alpha$ Syn regions mediating its high affinity interactions with MCIPs, we incubated synthetic peptide arrays containing  $\alpha$ Syn decamers covering its entire sequence and positionally shifted by one residue with Fluos-**2e** (Figure 5a, Supporting Figure S21).

We identified 3 clusters of strong binding decamers: one localized within the N-terminal segment  $\alpha$ Syn(1–14), a

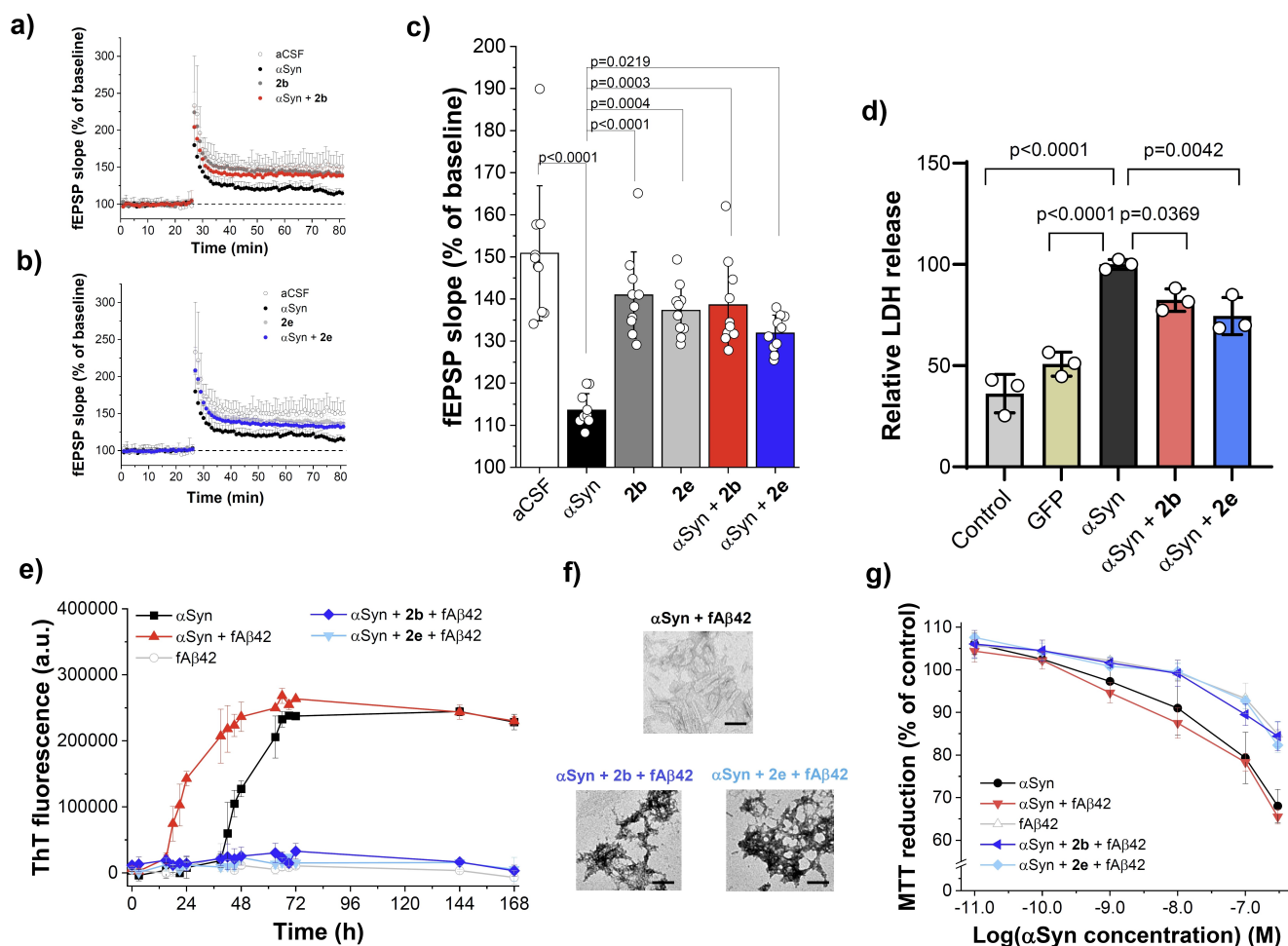


**Figure 4.** MCIPs ameliorate  $\alpha$ Syn-mediated synaptic damage in mouse brains ex vivo (a–c), suppress  $\alpha$ Syn cytotoxicity in  $\alpha$ Syn overexpressing human postmitotic dopaminergic neurons (d), and block cross-seeding of  $\alpha$ Syn amyloid self-assembly by  $\beta$ A42 fibrils (fA $\beta$ 42) (e–g). a–c) Suppression of  $\alpha$ Syn oligomer-induced LTP impairment in murine hippocampal slices ex vivo by **2b** and **2e**. a, b) Time course of synaptic transmission (fEPSP, field excitatory postsynaptic potential) after treatment with artificial cerebrospinal fluid (aCSF) medium (buffer control),  $\alpha$ Syn oligomers (175 nM), **2b** (a) or **2e** (b) alone (1.75  $\mu$ M), and  $\alpha$ Syn oligomers/**2b** (a) or **2e** (b) mixture (1/10) as indicated; data means ( $\pm$ SD), from  $n = 10$  samples/treatments each. c) LTP values; bars show the averages from the last 10 min of recording; data means ( $\pm$ SD),  $n = 10$  for each group; p-values as indicated; calculated using non-parametric testing with Mann-Whitney U-tests or a Kruskal-Wallis test. (d) Suppression of  $\alpha$ Syn-mediated toxicity in  $\alpha$ Syn overexpressing human postmitotic dopaminergic LUHMES neurons by **2b** and **2e** (10 nM) measured by LDH release. Grey column (control): untransduced cells; dark yellow column (GFP): cells transduced with GFP (control for virus); black column ( $\alpha$ Syn):  $\alpha$ Syn overexpressing cells without treatment; red column ( $\alpha$ Syn + **2b**):  $\alpha$ Syn overexpressing cells treated with **2b**; blue column ( $\alpha$ Syn + **2e**):  $\alpha$ Syn overexpressing cells treated with **2e**. Data means ( $\pm$ SEM) from 3 assays ( $n = 3$  each). Statistical significance was determined using one-way ANOVA, followed by Dunnett's multiple comparisons test; p-values as indicated. e–g) MCIPs block cross-seeding of  $\alpha$ Syn amyloid self-assembly by fA $\beta$ 42. Fibrillogenesis of  $\alpha$ Syn (3  $\mu$ M) alone or cross-seeded by fA $\beta$ 42 (20%) alone or with **2b** and **2e** (1/1) determined by ThT binding; data of fA $\beta$ 42 seeds (0.6  $\mu$ M) is also shown for comparison; data means ( $\pm$ SD), 3 assays (3 wells each) (e); TEM images of 7 day-aged solutions from (e) (scale bars, 100 nm) (f); PC12 cell viability after treatment with 7 day-aged solutions from (e) determined by the MTT reduction assay (means ( $\pm$ SD), 3 assays (3 wells each)) (g). P values  $< 0.05$  were considered significant.

2<sup>nd</sup> one within  $\alpha$ Syn(34–52), and a 3<sup>rd</sup> one within  $\alpha$ Syn(87–105) (Figure 5a, Supporting Figure S21). The results of the peptide array studies were confirmed and quantified by fluorescence spectroscopic titrations which revealed nanomolar app.  $K_{dS}$  for the interactions of **2e** and **2b** with all 3  $\alpha$ Syn segments (Figure 5b–d, Supporting Figure S22, Table 2). This data showed that the high affinity binding of MCIPs to  $\alpha$ Syn is mediated via the 3  $\alpha$ Syn regions  $\alpha$ Syn(1–14),  $\alpha$ Syn(34–52), and  $\alpha$ Syn(87–105).

Because MCIPs might mimic IAPP sites mediating its cross-interactions with  $\alpha$ Syn, we hypothesized that they might interact with the same/similar  $\alpha$ Syn regions as IAPP which could underlie their potent inhibitory activity on IAPP-mediated cross-seeding. To address this, the  $\alpha$ Syn peptide array was incubated with Fluos-IAPP. We identified 3 major binding clusters corresponding to  $\alpha$ Syn(1–13),  $\alpha$ Syn(34–46), and  $\alpha$ Syn(87–104) and a weaker one within the NAC region corresponding to  $\alpha$ Syn(68–80) (Figure 5e, Supporting Figure S23). Importantly, the 3 major IAPP-

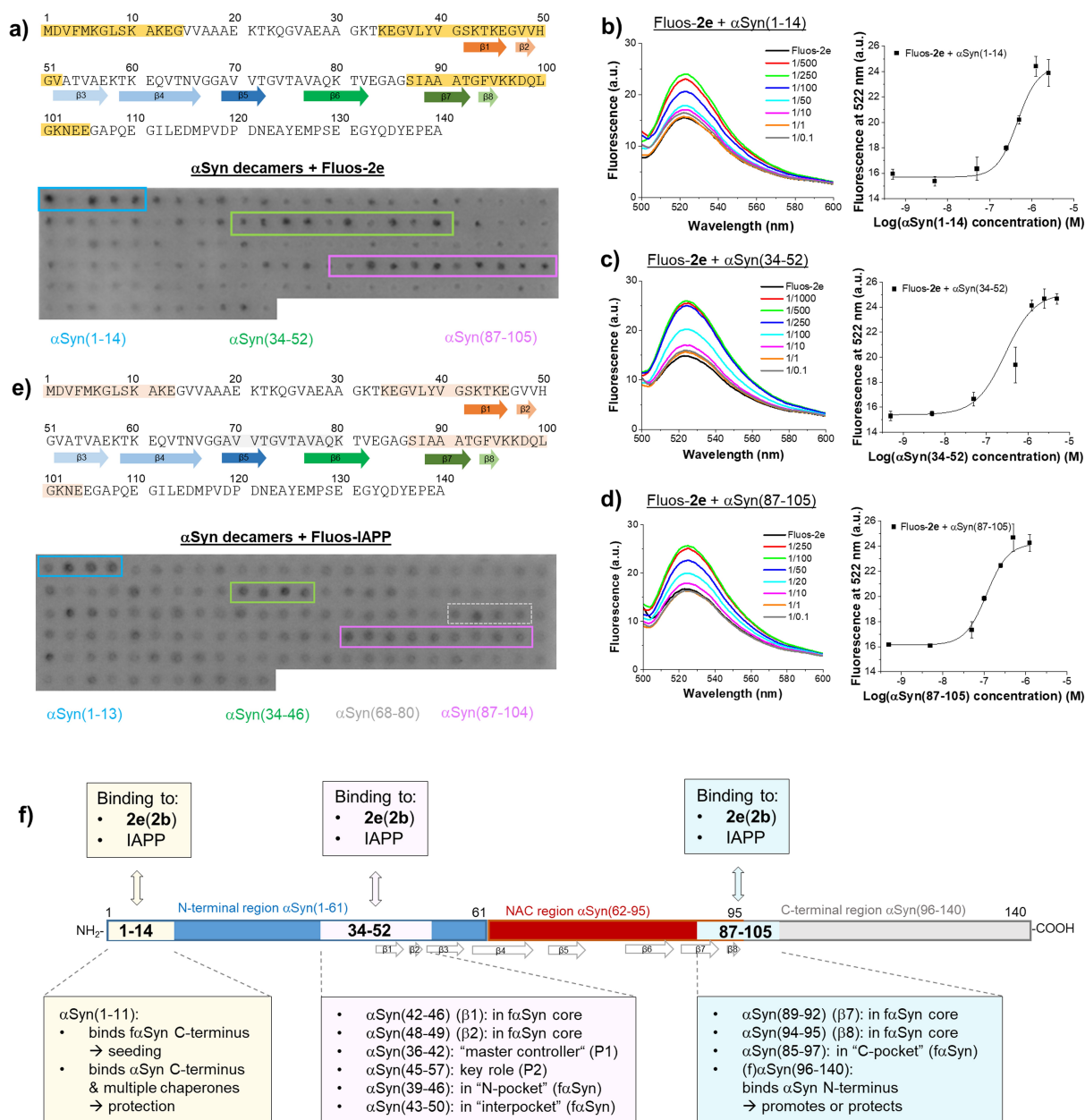


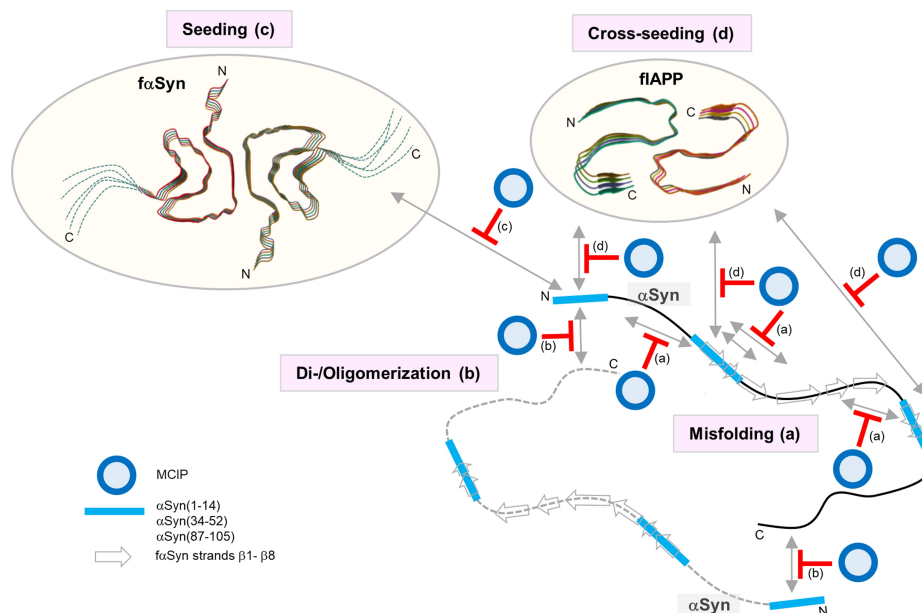
**Figure 5.** Identification of  $\alpha$ Syn segments mediating its interactions with MCIPs and IAPP by synthetic peptide arrays (a, e), determination of binding affinities by fluorescence spectroscopic titrations (b–d), and overview of key  $\alpha$ Syn interaction sites and related functions (f). a) Identification of key  $\alpha$ Syn regions interacting with **2e** using peptide arrays. Top,  $\alpha$ Syn sequence; identified **2e**-binding regions in orange rectangles as indicated; colored arrows indicate  $\beta$ -strands  $\beta$ 1– $\beta$ 8 in the *faSyn* fold of Guerreiro-Ferreira et al.<sup>[27]</sup> Bottom, peptide array containing  $\alpha$ Syn decamers following incubation with Fluos-**2e** (1  $\mu$ M) and bound peptide visualization by fluorescence; identified Fluos-**2e**-binding segments  $\alpha$ Syn(1–14),  $\alpha$ Syn(34–52), and  $\alpha$ Syn(87–105) in coloured rectangles. Array representative of 2 arrays synthesized in parallel and 2 independent incubations with Fluos-**2e** (Supporting Figure S21). b–d) Determination of app.  $K_d$ s of Fluos-**2e** interactions with identified **2e**-binding  $\alpha$ Syn segments by fluorescence spectroscopic titrations. Left, fluorescence emission spectra of Fluos-**2e** alone (5 nM) or with various molar ratios of  $\alpha$ Syn(1–14) (b),  $\alpha$ Syn(34–52) (c), and  $\alpha$ Syn(87–105) (d) (Fluos-**2e**/peptide as indicated). Spectra from 1 representative assay out of 3. Right, binding curves; data means ( $\pm$ SD) of 3 assays (see Table 2). e) Identification of key  $\alpha$ Syn regions interacting with IAPP using peptide arrays. Top,  $\alpha$ Syn sequence; IAPP-binding regions highlighted in pink (major) or grey (weaker); colored arrows as under (a).<sup>[27]</sup> Bottom, peptide array containing  $\alpha$ Syn decamers (as in (a)) following incubation with Fluos-IAPP (1  $\mu$ M) and visualization. Identified 3 major Fluos-IAPP-binding segments  $\alpha$ Syn(1–13),  $\alpha$ Syn(34–46), and  $\alpha$ Syn(87–104) in coloured rectangles (made by solid lines); weaker binding  $\alpha$ Syn(68–80): rectangle made by dashed lines. Array representative of two arrays synthesized in parallel and 2 independent incubations with Fluos-IAPP (Supporting Figure S23). f) Schematic overview of the 3 identified key  $\alpha$ Syn segments mediating its interactions with **2e**, **2b**, and IAPP and previously reported interactions & functions of related  $\alpha$ Syn sequence parts.<sup>[23b,27–28]</sup> White arrows indicate  $\beta$ -strands  $\beta$ 1– $\beta$ 8 in the *faSyn* fold of Guerreiro-Ferreira et al.<sup>[27]</sup>

binding  $\alpha$ Syn regions were nearly identical to the MCIP-binding ones which was consistent with our hypothesis. Furthermore, fluorescence spectroscopic titrations confirmed that the 3 major MCIP-binding  $\alpha$ Syn segments bind (f)IAPP as well and revealed that the affinities of their interactions with IAPP were very similar to the affinities of their interactions with **2b** and **2e** (Supporting Figure S24, S25, Table 2). Together, the above studies identified segments  $\alpha$ Syn(1–14),  $\alpha$ Syn(34–52), and  $\alpha$ Syn(87–105) as key sites of the high affinity interactions of  $\alpha$ Syn with both the MCIPs and IAPP.

Remarkably, the identified  $\alpha$ Syn segments mediating interactions with **2e**, **2b**, and IAPP localize in  $\alpha$ Syn regions which are well known for their crucial role in  $\alpha$ Syn amyloid self-assembly and related cell damage (Figure 5f).<sup>[27–28]</sup> Their amyloid modulatory functions have been suggested to be mediated by multi-pronged interactions with various parts of  $\alpha$ Syn and various other molecules (Figure 5f).<sup>[23b,27–28,29]</sup> For instance, the N-terminal region  $\alpha$ Syn(1–60) is known for its key role in  $\alpha$ Syn amyloidogenesis via self-assembly-promoting or -suppressing interactions e.g. with lipids, chaperones, and parts of  $\alpha$ (or  $\beta$ )Syn.<sup>[22a,28a–f,1,m,30]</sup> In this context, intermolecular interactions of  $\alpha$ Syn(1–11) or  $\alpha$ Syn(1–20) with the C-terminal part  $\alpha$ Syn(96–140) of  $\alpha$ Syn oligomers or fibrils were found to trigger  $\alpha$ Syn amyloidogenesis; by contrast, intramolecular interactions between N- and C-termini of  $\alpha$ Syn monomers may protect from aggregation.<sup>[28a,b,d,e,m]</sup> In addition,  $\alpha$ Syn(36–42), known as “P1”, has been suggested to be a “master controller” of  $\alpha$ Syn amyloid self-assembly while  $\alpha$ Syn(45–57), known as “P2” or “pre-NAC” region ( $\alpha$ Syn-

(45–56)), is an additional key regulator of  $\alpha$ Syn amyloid self-assembly.<sup>[28f,k]</sup> Also, parts of  $\alpha$ Syn(34–52) were found to mediate  $\alpha$ Syn interactions with diverse amyloid modulators including designed peptides/proteins and small molecules.<sup>[8b,c,28g,29b]</sup> Finally, MCIP- and IAPP-binding segments  $\alpha$ Syn(34–52) and  $\alpha$ Syn(87–105) are located in 3 out of 4 recently identified small molecule binding pockets of  $\alpha$ Syn.<sup>[28i]</sup>

The potent inhibitor function of the MCIPs on both self- and IAPP cross-seeded  $\alpha$ Syn amyloid self-assembly is thus likely mediated by high affinity interactions with  $\alpha$ Syn via 3  $\alpha$ Syn segments which localize in regions known for their crucial role in  $\alpha$ Syn amyloid self-assembly and were here identified as key sites of its cross-interactions with IAPP as well (Scheme 2). Together with previous results by others, our findings suggest that MCIPs’ multi-site binding to  $\alpha$ Syn blocks interactions underlying  $\alpha$ Syn misfolding cytotoxic di-/oligomerization, (self-)seeding, and IAPP-mediated mediated cross-seeding and support the suggestion that multi-site targeting of  $\alpha$ Syn could be a key requirement for effective anti-amyloid function (Scheme 2).<sup>[22a,23b,27–28]</sup> Our results also suggest that MCIPs’ ability to mimic IAPP sites mediating IAPP/ $\alpha$ Syn cross-interactions accounts for multi-site targeting of  $\alpha$ Syn and support the notion that common molecular recognition features of A $\beta$ , IAPP, and  $\alpha$ Syn exist which can be exploited to develop multi-functional anti-amyloid molecules.<sup>[7d,11,23b,29b,32]</sup>



**Scheme 2.** Schematic overview of proposed multi-site targeting mechanism of inhibitory function of MCIPs on both self- and flAPP-cross-seeded  $\alpha$ Syn amyloid self-assembly. High affinity binding of MCIPs (blue circles) to the three identified  $\alpha$ Syn key sites blocks crucial interactions of  $\alpha$ Syn with  $\alpha$ Syn, fuSyn, and (f)IAPP found previously ((a)–(c))<sup>[22a,23b,27–28]</sup> or in this work (d) to underlie  $\alpha$ Syn misfolding (a), di-/oligomerization (b), seeding by fuSyn (c), and cross-seeding by flAPP (d) (events in pink rectangles).  $\alpha$ Syn monomers are shown in intrinsically disordered state; blue bars, identified  $\alpha$ Syn key segments; grey arrows,  $\beta$ -strand forming regions in fuSyn fold of Guerrero-Ferreira et al.<sup>[27]</sup>; the fuSyn model is a modification of the fuSyn fold of Guerrero-Ferreira et al.,<sup>[27]</sup> the flAPP model is the flAPP fold of Roeder et al.<sup>[31]</sup>

## Conclusions

Here we show that the macrocyclic peptides **2b** and **2e**, designed to mimic IAPP self-/cross-interaction sites and previously found to be potent inhibitors of amyloid self-assembly of IAPP and/or the amyloid- $\beta$  peptide ( $A\beta$ ) of Alzheimer's disease (AD), are nanomolar inhibitors of both self- and IAPP-cross-seeded amyloid self-assembly of  $\alpha$ Syn. Our results suggest that their anti-amyloid function is mediated by nanomolar affinity interactions with  $\alpha$ Syn via three  $\alpha$ Syn segments which are identified as key sites of both  $\alpha$ Syn self- and its cross-interactions with IAPP. Furthermore, we show that **2b** and **2e** are also able to block  $A\beta$ 42-mediated cross-seeding of  $\alpha$ Syn. Based on their broad spectrum amyloid inhibitor activity and additional drug-like properties, these macrocyclic peptides are promising leads for multifunctional anti-amyloid drugs in PD, T2D, AD, and their comorbidities and studies in animal models are now an important next step. In addition, the identified key  $\alpha$ Syn segments shall serve as valuable targets for the design of novel, multi-site targeting molecules as effective anti-amyloids in PD and related synucleinopathies.

## Acknowledgements

This work was supported by Deutsche Forschungsgemeinschaft (DFG, German Research Foundation) grant SFB1035 B06 to A.K. in the framework of Collaborative Research Center (CRC) SFB1035 (project number 201302640). R.F., J.B., G.H., and T.K. were funded by DFG under Germany's Excellence Strategy within the framework of the Munich Cluster for Systems Neurology (EXC 2145 SyNergy-ID 390857198). G.H. and T.K. were also funded by the JPND Consortium, SynOD „alpha-Synuclein OMICS to identify Drug-targets“ (funded by the Federal Ministry of Education and Research, BMBF, 01ED2405 A). S.H. was supported by a fellowship of the Studienstiftung des Deutschen Volkes e.V. We thank C. Peters and the late S. Weinkauff for help with TEM. We thank the Bavarian Center for Biomolecular Mass Spectrometry (BayBioMS) at TUM School of Life Science and the Mass Spectrometry facility of the TUM School of Natural Sciences for access to MALDI and ESI mass spectrometry and support. We thank K. Hille, J. Jekel, C. Kontos, and A. Calzi for mass spectrometry measurements. We thank K. Hille, A. Grammatikopoulos, A. Pena-Vaquero, A. Seidler, and J. Jekel for peptide synthesis and purification. We thank K. Tas, V. Armiento, K. Hille, and C. Kontos for contributions to the synthesis of the peptide arrays and C. Krammer, S. Gerra, and B. Yang for peptide array immobilization onto glass slides or development. We thank H. Ji and O. Gokce for anti-**2e** antibody-validation. We thank J. Buchner and other members of SFB1035 for valuable discussions and support. Open Access funding enabled and organized by Projekt DEAL.

## Conflict of Interest

Potential conflict of interest: A. Spanopoulou, L. Heidrich, J. Bernhagen, and A. Kapurniotu are co-inventors of a European Patent Application and an US Patent No. US 11, 498,943 (by TUM) related to the macrocyclic peptides of our manuscript and potential biomedical applications in AD and T2D. In addition, S. Hornung and A. Kapurniotu are co-inventors in a European Patent Application filled by TUM in 2024 related to the peptides of the manuscript and potential biomedical applications in PD, synucleinopathies, and comorbidities. The remaining authors declare no competing interests.

## Data Availability Statement

The data that support the findings of this study are available from the corresponding author upon reasonable request.

**Keywords:**  $\alpha$ -synuclein · protein-protein interactions · (cross-)seeding · self-assembly · amyloid inhibitor

- [1] a) P. C. Ke, R. Zhou, L. C. Serpell, R. Riek, T. P. J. Knowles, H. A. Lashuel, E. Gazit, I. W. Hamley, T. P. Davis, M. Fandrich, D. E. Otzen, M. R. Chapman, C. M. Dobson, D. S. Eisenberg, R. Mezzenga, *Chem. Soc. Rev.* **2020**, *49*, 5473–5509; b) F. Chiti, C. M. Dobson, *Annu. Rev. Biochem.* **2017**, *86*, 27–68.
- [2] a) H. A. Lashuel, C. R. Overk, A. Oueslati, E. Masliah, *Nat. Rev. Neurosci.* **2013**, *14*, 38–48; b) S. Neupane, E. De Cecco, A. Aguzzi, *J. Mol. Biol.* **2023**, *435*, 167930.
- [3] P. Westermark, A. Andersson, G. T. Westermark, *Physiol. Rev.* **2011**, *91*, 795–826.
- [4] a) D. Athauda, J. Evans, A. Wernick, G. Virdi, M. L. Choi, M. Lawton, N. Vijiaratnam, C. Girges, Y. Ben-Shlomo, K. Ismail, H. Morris, D. Grosset, T. Foltynie, S. Gandhi, *J. Mov. Disord.* **2022**, *37*, 1612–1623; b) C. M. Labandeira, A. Fraga-Bau, D. Arias Ron, E. Alvarez-Rodriguez, P. Vicente-Alba, J. Lago-Garma, A. I. Rodriguez-Perez, *Neural Regen. Res.* **2022**, *17*, 1652–1658; c) Y. Q. Lv, L. Yuan, Y. Sun, H. W. Dou, J. H. Su, Z. P. Hou, J. Y. Li, W. Li, *Transl. Neurodegener.* **2022**, *11*, 14.
- [5] a) I. Horvath, P. Wittung-Stafshede, *Proc. Natl. Acad. Sci. USA* **2016**, *113*, 12473–12477; b) T. Werner, I. Horvath, P. Wittung-Stafshede, *J. Parkinsons Dis.* **2020**, *10*, 819–830; c) L. Meng, Y. Li, C. Liu, G. Zhang, J. Chen, M. Xiong, L. Pan, X. Zhang, G. Chen, J. Xiong, C. Liu, X. Xu, L. Bu, Z. Zhang, Z. Zhang, *Prog. Neurobiol.* **2023**, *226*, 102462; d) I. Martinez-Valbuena, I. Amat-Villegas, R. Valenti-Azcarate, M. D. M. Carmona-Abellan, I. Marcilla, M. T. Tunon, M. R. Luquin, *Acta Neuropathol.* **2018**, *135*, 877–886.
- [6] a) F. Bassil, H. J. Brown, S. Pattabhiraman, J. E. Iwaszyk, C. M. Maghames, E. S. Meymand, T. O. Cox, D. M. Riddle, B. Zhang, J. Q. Trojanowski, V. M. Lee, *Neuron* **2023**, *111*, 3699; b) M. B. Fares, B. Maco, A. Oueslati, E. Rockenstein, N. Ninkina, V. L. Buchman, E. Masliah, H. A. Lashuel, *Proc. Natl. Acad. Sci. USA* **2016**, *113*, E912–921.
- [7] a) P. Joshi, M. Vendruscolo, *Adv. Exp. Med. Biol.* **2015**, *870*, 383–400; b) H. Lu, Q. Zhou, J. He, Z. Jiang, C. Peng, R. Tong, J. Shi, *Signal Transduct. Target Ther.* **2020**, *5*, 213; c) J. A. Wells, C. L. McClendon, *Nature* **2007**, *450*, 1001–1009; d) V. Armién-

- to, A. Spanopoulou, A. Kapurniotu, *Angew. Chem. Int. Ed. Engl.* **2020**, *59*, 3372–3384.
- [8] a) H. Grosso Jasutkar, S. E. Oh, M. M. Mouradian, *Pharmacol. Rev.* **2022**, *74*, 207–237; b) S. G. Allen, R. M. Meade, L. L. White Stenner, J. M. Mason, *Mol. Neurodegener.* **2023**, *18*, 80; c) S. Pena-Diaz, J. Garcia-Pardo, S. Ventura, *Pharmaceutica* **2023**, *15*.
- [9] a) A. A. Vinogradov, Y. Yin, H. Suga, *J. Am. Chem. Soc.* **2019**, *141*, 4167–4181; b) M. Muttenthaler, G. F. King, D. J. Adams, P. F. Alewood, *Nat. Rev. Drug Discovery* **2021**, *20*, 309–325; c) X. Ji, A. L. Nielsen, C. Heinis, *Angew. Chem. Int. Ed. Engl.* **2024**, *63*, e202308251; d) H. Zhang, S. Chen, *RSC Chem Biol* **2022**, *3*, 18–31.
- [10] D. Goyal, S. Shuaib, S. Mann, B. Goyal, *ACS Comb. Sci.* **2017**, *19*, 55–80.
- [11] A. Spanopoulou, L. Heidrich, H. R. Chen, C. Frost, D. Hrle, E. Malideli, K. Hille, A. Grammatikopoulos, J. Bernhagen, M. Zacharias, G. Rammes, A. Kapurniotu, *Angew. Chem. Int. Ed. Engl.* **2018**, *57*, 14503–14508.
- [12] E. Andreetto, E. Malideli, L. M. Yan, M. Kracklauer, K. Farbiarz, M. Tatarek-Nossol, G. Rammes, E. Prade, T. Neumuller, A. Caporale, A. Spanopoulou, M. Bakou, B. Reif, A. Kapurniotu, *Angew. Chem. Int. Ed. Engl.* **2015**, *54*, 13095–13100.
- [13] M. Bakou, K. Hille, M. Kracklauer, A. Spanopoulou, C. V. Frost, E. Malideli, L. M. Yan, A. Caporale, M. Zacharias, A. Kapurniotu, *J. Biol. Chem.* **2017**, *292*, 14587–14602.
- [14] a) L. M. Yan, A. Velkova, M. Tatarek-Nossol, E. Andreetto, A. Kapurniotu, *Angew. Chem. Int. Ed. Engl.* **2007**, *46*, 1246–1252; b) K. Tas, B. D. Volta, C. Lindner, O. El Bounkari, K. Hille, Y. Tian, X. Puig-Bosch, M. Ballmann, S. Hornung, M. Ortner, S. Prem, L. Meier, G. Rammes, M. Haslbeck, C. Weber, R. T. A. Megens, J. Bernhagen, A. Kapurniotu, *Nat. Commun.* **2022**, *13*, 5004; c) A. Velkova, M. Tatarek-Nossol, E. Andreetto, A. Kapurniotu, *Angew. Chem. Int. Ed. Engl.* **2008**, *47*, 7114–7118; d) L. M. Yan, A. Velkova, M. Tatarek-Nossol, G. Rammes, A. Sibaev, E. Andreetto, M. Kracklauer, M. Bakou, E. Malideli, B. Goke, J. Schirra, M. Storr, A. Kapurniotu, *Angew. Chem. Int. Ed. Engl.* **2013**, *52*, 10378–10383; e) P. Krotee, S. L. Griner, M. R. Sawaya, D. Cascio, J. A. Rodriguez, D. Shi, S. Philipp, K. Murray, L. Saelices, J. Lee, P. Seidler, C. G. Glabe, L. Jiang, T. Gonen, D. S. Eisenberg, *J. Biol. Chem.* **2018**, *293*, 2888–2902.
- [15] a) E. Andreetto, L. M. Yan, M. Tatarek-Nossol, A. Velkova, R. Frank, A. Kapurniotu, *Angew. Chem. Int. Ed. Engl.* **2010**, *49*, 3081–3085; b) J. J. Wiltzius, S. A. Sievers, M. R. Sawaya, D. Eisenberg, *Protein Sci.* **2009**, *18*, 1521–1530.
- [16] M. R. Eftink, in *Methods in Enzymology: Fluorescence Spectroscopy*, Vol. 278 (Eds.: L. Brand, M. L. Johnson), Academic Press, San Diego, **1997**, pp. 221–257.
- [17] E. Andreetto, L. M. Yan, A. Caporale, A. Kapurniotu, *ChemBioChem* **2011**, *12*, 1313–1322.
- [18] M. Tornquist, T. C. T. Michaels, K. Sanagavarapu, X. Yang, G. Meisl, S. I. A. Cohen, T. P. J. Knowles, S. Linse, *Chem. Commun.* **2018**, *54*, 8667–8684.
- [19] L. M. Yan, M. Tatarek-Nossol, A. Velkova, A. Kazantzis, A. Kapurniotu, *Proc. Natl. Acad. Sci. USA* **2006**, *103*, 2046–2051.
- [20] Z. Niu, E. Prade, E. Malideli, K. Hille, A. Jussupov, Y. G. Mideksa, L. M. Yan, C. Qian, M. Fleisch, A. C. Messias, R. Sarkar, M. Sattler, D. C. Lamb, M. J. Feige, C. Camilloni, A. Kapurniotu, B. Reif, *Angew. Chem. Int. Ed. Engl.* **2020**, *59*, 5771–5781.
- [21] a) S. T. Kumar, S. Donzelli, A. Chiki, M. M. K. Syed, H. A. Lashuel, *J. Neurochem.* **2020**, *153*, 103–119; b) N. Lorenzen, S. B. Nielsen, A. K. Buell, J. D. Kaspersen, P. Arosio, B. S. Vad, W. Paslawski, G. Christiansen, Z. Valnickova-Hansen, M. Andreasen, J. J. Enghild, J. S. Pedersen, C. M. Dobson, T. P. Knowles, D. E. Otzen, *J. Am. Chem. Soc.* **2014**, *136*, 3859–3868; c) B. Fauvet, M. K. Mbefo, M. B. Fares, C. Desobry, S. Michael, M. T. Ardah, E. Tsika, P. Coune, M. Prudent, N. Lion, D. Eliezer, D. J. Moore, B. Schneider, P. Aebischer, O. M. El-Agnaf, E. Masliah, H. A. Lashuel, *J. Biol. Chem.* **2012**, *287*, 15345–15364.
- [22] a) G. Fusco, S. W. Chen, P. T. F. Williamson, R. Cascella, M. Perni, J. A. Jarvis, C. Cecchi, M. Vendruscolo, F. Chiti, N. Cremades, L. Ying, C. M. Dobson, A. De Simone, *Science* **2017**, *358*, 1440–1443; b) R. Cascella, S. W. Chen, A. Bigi, J. D. Camino, C. K. Xu, C. M. Dobson, F. Chiti, N. Cremades, C. Cecchi, *Nat. Commun.* **2021**, *12*, 1814.
- [23] a) R. Kayed, E. Head, J. L. Thompson, T. M. McIntire, S. C. Milton, C. W. Cotman, C. G. Glabe, *Science* **2003**, *300*, 486–489; b) M. Chemerovski-Glikman, E. Rozentur-Shkop, M. Richman, A. Grupi, A. Getler, H. Y. Cohen, H. Shaked, C. Wallin, S. K. Warmlander, E. Haas, A. Graslund, J. H. Chill, S. Rahimipour, *Chemistry* **2016**, *22*, 14236–14246.
- [24] a) M. J. Diogenes, R. B. Dias, D. M. Rombo, H. Vicente Miranda, F. Maiolino, P. Guerreiro, T. Nasstrom, H. G. Franquelim, L. M. Oliveira, M. A. Castanho, L. Lannfelt, J. Bergstrom, M. Ingelsson, A. Quintas, A. M. Sebastiao, L. V. Lopes, T. F. Outeiro, *J. Neurosci.* **2012**, *32*, 11750–11762; b) F. van Diggelen, D. Hrle, M. Apetri, G. Christiansen, G. Rammes, A. Tepper, D. E. Otzen, *PLoS One* **2019**, *14*, e0213663.
- [25] a) M. Hollerhage, J. N. Goebel, A. de Andrade, T. Hildebrandt, A. Dolga, C. Culmsee, W. H. Oertel, B. Hengerer, G. U. Hoglinger, *Neurobiol. Aging* **2014**, *35*, 1700–1711; b) M. Hollerhage, C. Moebius, J. Melms, W. H. Chiu, J. N. Goebel, T. Chakroun, T. Koeglsperger, W. H. Oertel, T. W. Rosler, M. Bickle, G. U. Hoglinger, *Sci. Rep.* **2017**, *7*, 11469.
- [26] F. Bassil, H. J. Brown, S. Pattabhiraman, J. E. Iwasyk, C. M. Maghames, E. S. Meymand, T. O. Cox, D. M. Riddle, B. Zhang, J. Q. Trojanowski, V. M. Lee, *Neuron* **2020**, *105*, 260–275 e266.
- [27] R. Guerrero-Ferreira, N. M. Taylor, D. Mona, P. Ringler, M. E. Lauer, R. Riek, M. Britschgi, H. Stahlberg, *eLife* **2018**, *7*.
- [28] a) S. D. Khare, P. Chinchilla, J. Baum, *Curr. Opin. Struct. Biol.* **2023**, *80*, 102579; b) X. Yang, B. Wang, C. L. Hoop, J. K. Williams, J. Baum, *Proc. Natl. Acad. Sci. USA* **2021**, *118*; c) J. K. Williams, X. Yang, T. B. Atieh, M. P. Olson, S. D. Khare, J. Baum, *J. Mol. Biol.* **2018**, *430*, 2360–2371; d) P. Kumari, D. Ghosh, A. Vanas, Y. Fleischmann, T. Wiegand, G. Jeschke, R. Riek, C. Eichmann, *Proc. Natl. Acad. Sci. USA* **2021**, *118*; e) R. P. McGlinchey, X. Ni, J. A. Shadish, J. Jiang, J. C. Lee, *Proc. Natl. Acad. Sci. USA* **2021**, *118*; f) C. P. A. Doherty, S. M. Ulamec, R. Maya-Martinez, S. C. Good, J. Makepeace, G. N. Khan, P. van Oosten-Hawle, S. E. Radford, D. J. Brockwell, *Nat. Struct. Mol. Biol.* **2020**, *27*, 249–259; g) E. A. Mirecka, H. Shaykhalishahi, A. Gauhar, S. Akgul, J. Lecher, D. Willbold, M. Stoldt, W. Hoyer, *Angew. Chem. Int. Ed. Engl.* **2014**, *53*, 4227–4230; h) E. D. Agerschou, P. Flagmeier, T. Saridakis, C. Galvagnion, D. Komnig, L. Heid, V. Prasad, H. Shaykhalishahi, D. Willbold, C. M. Dobson, A. Voigt, B. Falkenburger, W. Hoyer, A. K. Buell, *eLife* **2019**, *8*; i) Y. Tao, W. Xia, Q. Zhao, H. Xiang, C. Han, S. Zhang, W. Gu, W. Tang, Y. Li, L. Tan, D. Li, C. Liu, *Nat. Chem. Biol.* **2023**, *19*, 1235–1245; j) B. Li, P. Ge, K. A. Murray, P. Sheth, M. Zhang, G. Nair, M. R. Sawaya, W. S. Shin, D. R. Boyer, S. Ye, D. S. Eisenberg, Z. H. Zhou, L. Jiang, *Nat. Commun.* **2018**, *9*, 3609; k) S. M. Ulamec, R. Maya-Martinez, E. J. Byrd, K. M. Dewison, Y. Xu, L. F. Willis, F. Sobott, G. R. Heath, P. van Oosten-Hawle, V. L. Buchman, S. E. Radford, D. J. Brockwell, *Nat. Commun.* **2022**, *13*, 4986; l) G. Fusco, A. De Simone, T. Gopinath, V. Vostrikov, M. Vendruscolo, C. M. Dobson, G. Veglia, *Nat. Commun.* **2014**, *5*, 3827; m) B. M. Burmann, J. A. Gerez, I. Matecko-Burmann, S. Campioni, P. Kumari, D.

- Ghosh, A. Mazur, E. E. Aspholm, D. Sulskis, M. Wawrzyniuk, T. Bock, A. Schmidt, S. G. D. Rudiger, R. Riek, S. Hiller, *Nature* **2020**, 577, 127–132.
- [29] a) H. Shaykhalishahi, A. Gauhar, M. M. Wordehoff, C. S. Gruning, A. N. Klein, O. Bannach, M. Stoldt, D. Willbold, T. Hard, W. Hoyer, *Angew. Chem. Int. Ed. Engl.* **2015**, 54, 8837–8840; b) H. Shaykhalishahi, E. A. Mirecka, A. Gauhar, C. S. Gruning, D. Willbold, T. Hard, M. Stoldt, W. Hoyer, *Chem-BioChem* **2015**, 16, 411–414.
- [30] E. Cholak, K. Bugge, A. Khondker, K. Gauger, E. Pedraz-Cuesta, M. E. Pedersen, S. Bucciarelli, B. Vestergaard, S. F. Pedersen, M. C. Rheinstadter, A. E. Langkilde, B. B. Krage-lund, *FASEB J.* **2020**, 34, 7462–7482.
- [31] C. Roder, T. Kupreichyk, L. Gremer, L. U. Schafer, K. R. Pothula, R. B. G. Ravelli, D. Willbold, W. Hoyer, G. F. Schroder, *Nat. Struct. Mol. Biol.* **2020**, 27, 660–667.
- [32] A. Frydman-Marom, R. Shaltiel-Karyo, S. Moshe, E. Gazit, *Amyloid* **2011**, 18, 119–127.

Manuscript received: November 23, 2024

Accepted manuscript online: January 17, 2025

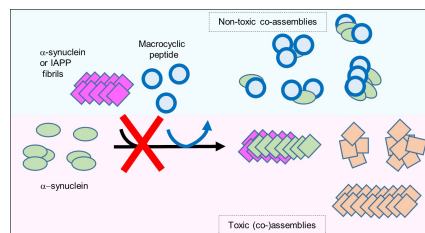
Version of record online: ■■, ■■

## Research Article

## Amyloid Inhibitors

S. Hornung, D. P. Vogl, D. Naltsas,  
B. D. Volta, M. Ballmann, B. Marcon,  
M. M. K. Syed, Y. Wu, A. Spanopoulou,  
R. Feederle, L. Heidrich, J. Bernhagen,  
T. Koeglsperger, G. U. Höglinger,  
G. Rammes, H. A. Lashuel,  
A. Kapurniotu\* e202422834

Multi-Targeting Macrocylic Peptides as  
Nanomolar Inhibitors of Self- and Cross-  
Seeded Amyloid Self-Assembly of  $\alpha$ -Synu-  
clein



Cross-seeding of  $\alpha$ -synuclein ( $\alpha$ Syn) amyloid self-assembly by islet amyloid polypeptide (IAPP) has been suggested to link type 2 diabetes to Parkinson's disease. Here we show that designed multi-targeting macrocyclic peptides pre-

viously found to inhibit IAPP and/or Alzheimer's amyloid- $\beta$  peptide (A $\beta$ 40 (42)) are nanomolar inhibitors of both self- and IAPP-cross-seeded  $\alpha$ Syn amyloid self-assembly and promising leads for multifunctional anti-amyloid drugs.